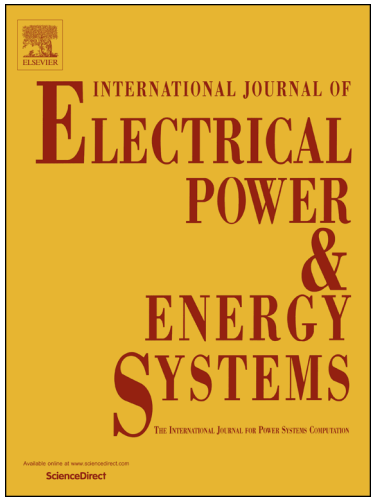

Strategy of Management of Storage Systems Integrated with Photovoltaic Systems for Mitigating the Impact on LV Distribution Network

Andrés Cortés, Javier Mazón, Julia Merino

PII: S0142-0615(18)30669-0
DOI: https://doi.org/10.1016/j.ijepes.2018.06.012
Reference: JEPE 4715

To appear in: *International Journal of Electrical Power and Energy Systems*

Received Date: 5 March 2018
Revised Date: 24 April 2018
Accepted Date: 1 June 2018

Please cite this article as: A. Cortés, J. Mazón, J. Merino, Strategy of Management of Storage Systems Integrated with Photovoltaic Systems for Mitigating the Impact on LV Distribution Network, *International Journal of Electrical Power and Energy Systems* (2018), doi: https://doi.org/10.1016/j.ijepes.2018.06.012

Strategy of Management of Storage Systems Integrated with Photovoltaic Systems for Mitigating the Impact on LV Distribution Network

Andrés Cortés[a,b]*, Javier Mazón[a], Julia Merino[b]
a Dept. of Electrical Engineering, University of the Basque Country, Bilbao, Spain
b TECNALIA, Derio, Spain

Abstract

This article presents an integrated storage management strategy with photovoltaic systems connected to the grid, to provide voltage regulation and losses reduction in the low voltage feeder, minimising the power supplied by the network upstream of the main transformer. A new control algorithm for battery energy storage systems (BESS) is presented embedding as a battery management algorithm for charging and discharging process. The charging of the storage system is defined by the optimization of the α_k coefficient to establish the value of charging threshold power, in a distributed manner, to maximise the use of photovoltaic systems. The discharging process occurs by a given σ coefficient. A standard network model from CIGRE was used for the validation of the management strategy. It was modified with real profiles of load and irradiance with a minute resolution to adapt it to the using of the quasi-static load flow in MATLAB/Simulink. As a result, by integrating 67% of PV along with 442 kWh of BESS with its management algorithm, power import from the grid decreases up to 49.3%.

Keywords— Battery management systems, energy storage, photovoltaic systems, power generation dispatch

1. Introduction

The recent advances obtained in the field of small-scale generation and electrical storage, involve changes in the way in which the generation and distribution of energy have been conceived in recent decades. Consequently, the expansion of distributed generation employing photovoltaic systems with storage leads to essential challenges in the planning, investment, operation and regulation of traditional electricity distribution systems [1, 2]. However, for interconnected systems, this type of generation implies a change in vision. The end user will be able to manage the energy produced, delivering it to the low voltage system, during periods of maximum demand or valley, using the strategies of demand shift and demand reduction [3]. This vision would allow, among other things, to decrease transmission and distribution losses, increase system slack and reduce dependence on the centralised system. Consequently, it is convenient to identify the technical interconnection conditions for these new generation and storage systems, in such a way that the levels of reliability established within the electrical system are maintained.

One of the undeniable characteristics of the electrical energy generated by the photovoltaic systems is that it is not dispatchable due to the intermittency and unpredictability of the primary source of energy. This makes difficult to predict the power that will be generated by the system in a specific moment of time, as verified [4, 5, 6]. This uncertainty associated with the dispatch by the photovoltaic system does not generate significant inconveniences when it is only a user that is generating electrical

*Corresponding author. Superior Technical School of Engineering of Bilbao, Alda. de Urquijo s/n, 48013 Bilbao
E-mail addresses: acortes024@ikasle.ehu.eus, javier.mazon@ehu.eus (Javier Mazón), julia.merino@tecnalia.com (Julia Merino)

energy from this source. However, when it is no longer a single user, but multiple users within the electrical system injecting power from non-manageable sources located at scattered points in the network, this uncertainty is significantly affected. The most discussed topics are related to the generated power fluctuations, voltage instability and frequency deviations, imbalances, among others [7, 8, 9, 10, 29]. However, this impact on the network can be mitigated by the integration of energy storage systems in optimal points of the electric network. However, it is necessary to evaluate the amount of energy that should be stored and integrated into the network [11, 12], to mitigate these disturbances by performing the optimal dimensioning of the associated storage. For instance, Ref. [29] presents real applications of BESS, since 2011 to 2016, to balancing load peaks and valleys, frequency regulation, ramping, energy time shift, and voltage support among other by incorporating renewable generation.

Considering the high temporal intermittency associated with generation and limits on storage size the storage capacity is usually calculated only for short-term supply as work in [8, 13]. Besides, the optimal size and location of energy storage can be considered as support to the operational planning of the system with the massive insertion of photovoltaic systems, to maintain the power quality and reliability of the electrical system [14, 15]. Therefore, battery energy storage can be considered as a feasible solution to effectively get a reliable and safe power system based on PV generation. Then an analysis of the references found that address the problem of battery charging/discharging strategies that are integrated with PV is presented.

Thus, in Ref. [7] a control method in a DC topology for state-of-charge and battery charge/discharge is proposed to ensure efficient performance and safe operation of the storage system in combination with PV generation. The effects of the Active Demand-Side Management (ADSM) and storage systems for a single user in the amount of consumed local electrical energy is studied in Ref. [10] through a real installation of PV generation, lead-acid batteries, controllable appliances and smart metering. Moreover, in Ref. [14] a decentralised storage management strategy based on voltage sensitivity analysis, identifies a common power threshold that triggers the ESSs activation in the feeder to effectuate voltage support in low-voltage residential feeders with high PV capacity installed. In Ref. [17] a power management strategy is proposed for solving the cooperative operation of the energy storage systems and PV units in a multi-master micro-grid structure when local loads power demand changed. Additionally, an energy management strategy based on stochastic dynamic programming for a smart home with a plug-in electric vehicle as energy storage system and PV array is developed in Ref. [27]. Also, an optimisation framework based on convex programming for efficient energy management and components sizing of a smart home with battery energy storage, plug-in electric vehicles and PV arrays is presented in [28]. Furthermore, an active-power management scheme for the control of centralised battery energy-storage systems for large PV capacity firming and energy time shift is developed in Ref. [31]. On the other hand, Ref. [32] proposes an energy management system as a low-pass filtering algorithm with variable time constant which focuses on the power-sharing between the battery and supercapacitor due to PV power fluctuations with two optimisation objectives: energy loss and state-of-charge. Finally, in Ref. [33] is presented an energy management and control system for laboratory scale isolated

microgrid based on hybrid energy resources such as wind, solar, and battery storage mainly to keep a constant DC-link voltage under various loads and supply conditions.

In most of the related literature, few articles deal with multiple BESS+PV in a decentralised manner. However, these works do not consider the simultaneous activations of the BESS to provide power losses reduction and voltage support. In this sense, this article presents a new control algorithm for battery energy storage systems (BESS), embedding as a battery management algorithm for charging and discharging process based on the PV power generation and load behaviour. This approach demonstrates through a typical network that the impact associated with the growth of photovoltaic generation is clearly mitigated with an intelligent control strategy for the storage. For this study, multiple simulation cases have been carried out on a CIGRE standard low voltage distribution network [9], where photovoltaic generation systems with battery storage (PV+BESS) have been incorporated in different nodes. The objective is to assess the impact that its operation will cause in the planning of low voltage networks, before a future massification of this type of systems.

In Section 2 the topology of the PV+BESS system and its grid-connected operating modes are described. In Section 3 an overview of the test grids, the definition of the mathematical models of the demand, the photovoltaic generator and the storage system, together with the intelligent management strategy are shown. In Section 4 the results obtained from five case studies evaluated on the selected distribution network are presented. In Section 5 the conclusions, summary of contributions and hints on future works are presented.

2. The configuration of the PV+BESS

Fig. 1 presents a topology based on the coupling at the AC side, in which the photovoltaic generation and storage system work independently. As a result, this configuration presents the complexity of synchronism in its operation and, besides, the photovoltaic system does not allow charging the storage system directly, which reduces the energy efficiency of the whole. However, this does not limit the advantage of adjusting the operating parameters of the storage set depending on the photovoltaic generation system, as demonstrated in [16,17]. In this way, the energy balance of the electrical system is managed by the aggregation of PV+BESS, according to the instantaneous energy demand.

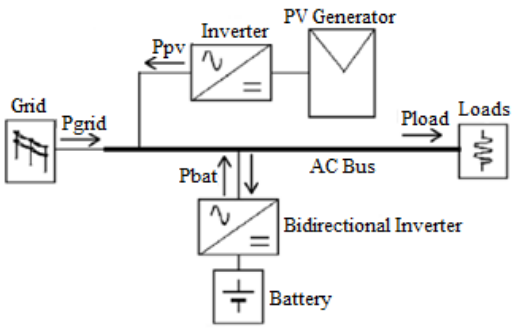

Fig. 1. Configuration of the PV+BESS

From the customer's point of view, the best benefit is to minimise the cost of the energy consumed from the network. Based on this consideration, and the model presented in

Fig. 1, if the user's daily load profile is known, it is possible to determine an optimal daily operation pattern from the network's point of view, as well as for the user. Consequently, the daily operation of the PV+BESS could be divided into four modes of operation, depending in the period of the day, as shown in Table 1.

Table 1
Proposed operation modes for PV+BESS

Mode	Period	Operating condition
1	Valley	From midnight to dawn, the photovoltaic system is inactive, and the storage system does not have enough energy to meet the demand. Therefore, the necessary energy will be imported from the grid.
2	Low irradiance	During the first hours of the morning, the photovoltaic energy is present, but not enough to charge the batteries and contribute to the demand; the network supplies the necessary energy.
3	High irradiance	From the end of the morning until mid-afternoon, the energy of the PV system is sometimes higher than that demanded by the load, so a limit is established on the power output of the PV generator, for which the storage system must enter to charge.
4	Discharging	From the end of the afternoon until midnight, the energy of the network is reduced to a minimum, since the demand is met by the photovoltaic generator and the initial discharge of the storage system. As the photovoltaic energy gradually decreases to zero, a percentage of the demand is finally supplied by the batteries and the remainder by the network.

Therefore, to avoid the PV energy spills during high irradiance periods, it has been established that the storage system can only be charged with the energy from the photovoltaic system, so that it can be used at night, minimising the contribution by of the network (Mode 3). Therefore, the instantaneous energy balance of the system is shown in (1):

$$E_{grid(t)} = E_{load(t)} - E_{PV(t)} - E_{bat(t)} \quad (1)$$

Where $E_{grid\ (t)}$, represents the electrical energy imported from the grid; $E_{Load\ (t)}$, is the total demand; $E_{PV\ (t)}$, is the energy contributed by the photovoltaic generation, and $E_{bat\ (t)}$, is the stored energy in the storage system.

3. System modelling and energy management system

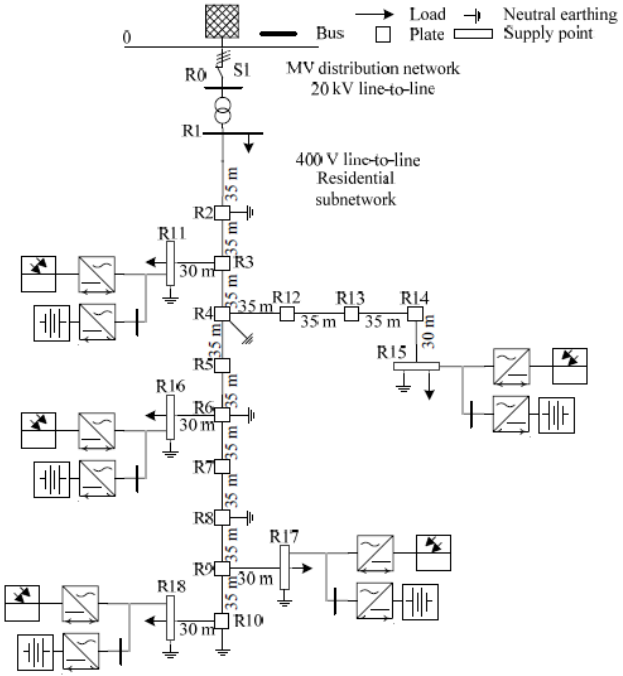

Fig. 2. LV distribution network model adapted from [9]

3.1. LV distribution system

A low voltage distribution network (LV) representative of a real European electrical system, proposed by CIGRE, was simulated with Simulink. The network comprises three load feeders: residential, industrial and commercial. However, the present study was developed on the residential branch of Fig. 2 where it has been installed the PV+BESS assemblies at the domestic level. The detailed information of the distribution system is shown in [9].

3.2. Demand Characterization

The selected demand profile is based on average annual energy consumption of 3370 kWh/year [18], for a typical house in the Basque Country. The annual normalised profile applicable to consumers with an installed electrical power lower than 10 kW according to regulation [19] was taken as a reference, to determine the behaviour of the demand. Because load varies by a considerable amount throughout the year, it was taken as a reference, the normalised load data between January and July [19] multiplied by the average energy consumption to represent the typical in winter and summer seasons. This evaluation was conducted by using a boxplot[1] representation to show the hourly variation per day of such power demand for January and July as shown in Fig. 3.a and b. Both months exhibit significant variability in the second quartile group of data during the first hours of the morning until noon, as well as after mid-afternoon until midnight by cause of the changes of people routines; some slight variations are perceived during the early morning due to the low human activity.

[1] **Boxplot:** The median marks the midpoint of the data and is represented by the line that divides the box into two parts. The box represents the middle 50% of scores for the group in an upper and lower bound which is referred to as the inter-quartile range. The upper and lower lines are known as whiskers, and those represent scores outside the middle 50%. Extreme data points are known as outliers and are represented by + signs.

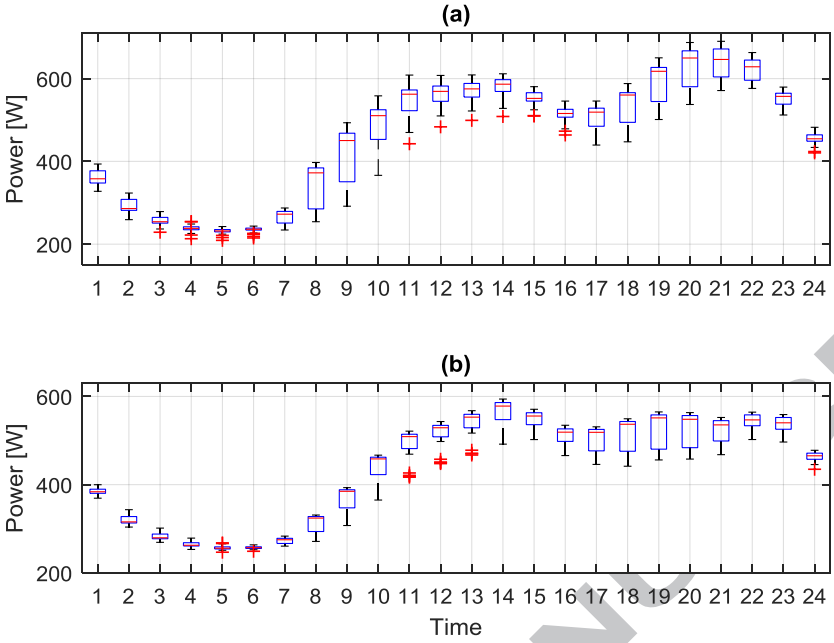

Fig. 3. a) Statistical hourly data of demand profile for winter scenario for a typical user in the Basque Country, b) Statistical hourly data of demand profile for summer scenario for a typical user in the Basque Country; both profiles are based on the data extracted from [19] for January and July, respectively.

In this way, the median of the hourly demand for the winter and summer scenarios was extracted, evaluated in a 1-minute integration step, to observe in detail the instantaneous load variations. For this, the trigonometric interpolation method was used, due to the high degree of precision [20], and the direct application of the discrete Fourier transform (DFT) on the sampled data at specific time intervals.

Thus, applying the DFT to the data of the median of the hourly demand for winter and summer (Fig. 3.a and b), analysed from [19], we obtain a trigonometric polynomial of 2x11 terms of cosine and sine for each scenario of demand.

Table 2
Load parameters for the LV network model

Node	P_{Summer} [kW]	P_{Winter} [kW]	N_{users}	PF
R11	11.09	14.37	22	0.95
R15	38.32	49.65	76	0.95
R16	40.34	52.27	80	0.95
R17	25.72	33.32	51	0.95
R18	34.29	44.43	68	0.95

On the other hand, Table 2 shows the coincident peak power values for the summer and winter demand of the set of users in each loading node, according to [9]. These are the result of scaling the median of the load curve of Fig. 3.a, and b on each node of the network. Note that these powers are the result of having applied the coincidence factor defined in (2).

$$\mathrm{CF} = 0.6 \cdot \left(1 + \frac{1}{N_{users}}\right) \tag{2}$$

From the power factor defined in Table 2, and the instantaneous active power value of each load profile in every node (P_{load}), the reactive power of the load (Q_{load}) for such instant is calculated from (3), considering the power factor (pf). The above will allow quantifying the magnitude of the current for each node, according to (4), as a function of the apparent power (S_{load}) and the positive sequence voltage (V_1) at the point of common coupling (*PCC)* as defined in (5).

$$\mathrm{Q_{load}} = P_{load} \cdot \sqrt{\frac{1}{pf^{\,2}} - 1} \tag{3}$$

$$\mathrm{S_{load}} = \frac{3}{2} \cdot \left(V_1 \cdot I^{*}\right) \tag{4}$$

$$V_1 = \frac{1}{3} \cdot \left(V_{AB} - a^2 \cdot V_{BC}\right) \tag{5}$$

3.3. PV system model and meteorological data

Classical approaches result in reasonable approximations of the expected parameters such as the maximum power point voltage and the maximum power point current to calculates the PV power as presented in Ref. [4]. Taking this into account, the hourly output power of the photovoltaic generator, P_{PV}, can be evaluated through (6) considering an area of PV modules, A_{PV}, with a global irradiance G_{Global} (W/m^2), and taking into account that the efficiency of the installation, η_{PV}, decreases due to the degradation of the PV modules [6].

$$P_{\mathrm{PV}} = \eta_{PV} \cdot A_{PV} \cdot G_{Global} \tag{6}$$

So that the required surface of the PV system for a peak power under standard conditions, P_{STC} (i.e., the nominal power of the PV array as shown in Table 6), is determined according to the module efficiency, η_{panel}, and to the irradiance under standard conditions, G_{STC} (1 kW/m^2). The above is formulated in (7).

$$A_{\mathrm{PV}} = \frac{P_{STC}}{\eta_{panel} \cdot G_{STC}} \tag{7}$$

According to [11], the overall efficiency of the PV system depends on the reference efficiency of the module, η_{panel}, the efficiency of the power conditioner (up to 1 if the adjustment to the maximum power point tracking curve is perfect), η_{pc}, a factor that considers the decrease in efficiency due to the effect of temperature, η_{temp}, and the efficiency of the inverter, η_{inv}, as defined in (8).

$$\eta_{PV} = \eta_{panel} \cdot \eta_{pc} \cdot \eta_{temp} \cdot \eta_{inv} \tag{8}$$

On the other hand, the efficiency of the PV module decreases linearly concerning the condition of the reference temperature of 25°C, $T_{cell,ref}$ [2], and is influenced by the efficiency coefficient of the module, β, which is assumed as a constant that varies from 0.004 to 0.006 1/°C for the silicon cells [2], as specified in (9).

$$\eta_{temp} = \left[1 - \beta \cdot \left(T_{cell} - T_{cell,ref}\right)\right] \tag{9}$$

Where the temperature of the cell of the module, T_{cell} is determined in (10) from the ambient temperature, $T_{environment}$, and the normal operating cell temperature, *NOCT*; given in Celsius degree.

$$T_{cell} = T_{enviroment} + \left(\frac{NOCT - 20}{800}\right) \cdot G_{Global} \tag{10}$$

The magnitude of the active power of each PV generator is obtained from the parameters contained in Table 4 and Table 6. It is also considered that the system operates with a unit power factor. On the other hand, the meteorological database in [21] for Bilbao city was used to extract the global irradiance and ambient temperature data. These data were used to evaluate statistically the hourly profile per day of the available solar resource and the ambient temperature associated with it, for January and June using a boxplot representation as displayed in Fig. 4.a and b along with Fig. 5.a and b, respectively. The median of the results of the data were used to test the PV model described in equations (6) to (10) for the winter and summer season.

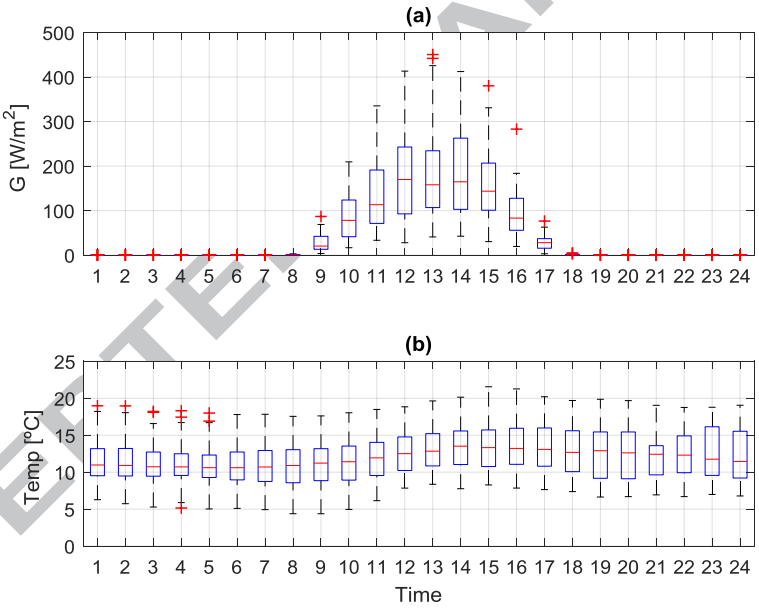

Fig. 4. a) Statistical daily profile of irradiance for winter scenario, b) Statistical daily profile of temperature for winter scenario; both profiles are based on the data extracted from [21] for January in Bilbao.

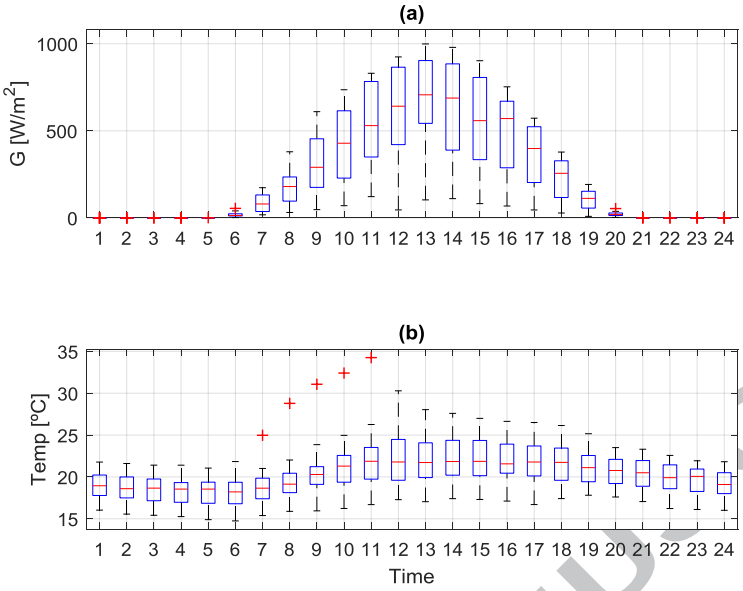

Fig. 5. a) Statistical daily profile of irradiance for summer scenario, b) Statistical daily profile of temperature for winter scenario; both profiles are based on the data extracted from [21] for July in Bilbao.

3.4. BESS model

In Ref. [22] different mathematical models are presented that define the behaviour and performance of batteries. However, all these models analyse the batteries from their DC nature from a series of parameters, some of them quite complex to estimate. However, based on the criteria that affect the performance of the batteries, such as the state of charge (*SOC*), the depth of discharge (*DOD*) and the storage capacity ($E_{bat(t)}$), a model has been defined to evaluate the discrete dynamics of the battery according to [3, 30, 34]. This model operates in a general manner based on these factors for regular lead-acid [3] or Li-ion batteries [27, 28], seen in terms of power, energy and efficiency.

Also, a bidirectional converter is necessary to condition the power during the charging and discharging process of the batteries. The efficiency of the converter, $\eta_{bat,\ inv}$, is assumed to be analogous for both processes. $P_{bat\ (t)}$ is used to denote the power exchanged with the AC bus, when the converter and batteries are treated as a unit [3, 13], which can be expressed from (11); where $P_{bat,ch(t)}$ is the charge power and $P_{bat,dis(t)}$ is the discharge power of the storage system over time, respectively.

$$P_{bat(t)} = \begin{cases} P_{bat,ch(t)} \cdot \eta_{bat,inv} & P_{bat(t)} < 0 \\ \dfrac{P_{bat,dis(t)}}{\eta_{bat,inv}} & otherwise \end{cases} \tag{11}$$

On the other hand, the *SOC* can be quantified from (12) and from the charge/discharge equations expressed from (13) to (15) based on the power interchange between sample times.

$$SOC_{(t)} = \frac{E_{bat(t+\Delta t)}}{E_{bat}^{\max}} \tag{12}$$

$$E_{bat(t0)}^{\min} = (1 - DOD) \cdot E_{bat}^{\max} \quad (13)$$

$$E_{bat,ch(t+\Delta t)} = E_{bat(t0)}^{\min} + \Delta t \cdot P_{bat,ch(t)} \cdot \eta_{bat,inv} \quad (14)$$

$$E_{bat,dis(t+\Delta t)} = E_{bat(t)} - \Delta t \cdot \frac{P_{at,dis(t)}}{\eta_{bat,inv}} \quad (15)$$

Thereby, in (12) the SOC will vary in each sample time interval (Δt) by the effect of the energy stored in the batteries at time t, $E_{bat(t+\Delta t)}$, up to reach the nominal capacity of the system, $E_{bat}^{\max}$ .On the other side, in (13) the minimum energy capacity of the storage system, $E_{bat}^{\min}$, will be determined by the maximum depth of discharge, *DOD*, and $E_{bat}^{\max}$. This last parameter is directly taken as input for (14) along with the product of the $P_{bat,ch(t)}$ and the converter efficiency in each sample time interval, Δt, to determine the energy charging to the battery at time t, $E_{bat,ch(t+\Delta t)}$. Similarly, in (15) the ratio between the $P_{bat,ch(t)}$ and the converter efficiency in each sample time interval, Δt, is subtracted from the last state of energy available in the battery at time t, $E_{bat(t)}$, to calculate the energy discharged from the battery at time t, $E_{bat,dis(t+\Delta t)}$.

The model described above can be applied to different types of batteries because the battery is seen as a unit where is possible to manage the energy stored within certain limits that assured the well-performance of the element as a function of the power interchange and the efficiency of the converter used. However, this study is based on the implementation of lead-acid batteries, due to their technological maturity and associated low cost for applications in renewable balancing as analysed in [29]. In this sense, typical desired values for *SOC* in this kind of batteries should be between the limits of $20\% \leq SOC \leq 100\%$, so that the integrity of the battery is maintained [10, 29, 30, 34]. Therefore, for this study it is defined that the *SOC* bounds will be $30\% \leq SOC \leq 100\%$ of the capacity of the battery which correspond to a *DOD* of 70%.

3.5. Energy management system algorithm

In the present study, the system developed aims to satisfy the demand for hourly energy thanks to the energy produced by the PV system or the energy stored in the battery system. The connection to the network works as a source of backup power if the PV+BESS cannot fully satisfy the demand of the users. For this, it is necessary to use an algorithm that allows carrying out the control of charging and discharging process of the storage group to optimise the consumption and generation of the installation at the PCC.

In this way, [14] proposes the activation of the storage system in the feeder from a threshold power, P_{th}, to optimise the operation of the system and mitigate the phenomena associated with conventional charging. For example, the BESS starts to charge as soon as the PV power surpasses the P_{load}, commonly at first hours in the morning, and stops at noon when the BESS will reach its SOC_{max}. This behaviour leads to deliver the energy excess to the grid. In this way, it is proposed to solve the modified function from [14] and express it as in (16) as an objective function which aim is the minimisation of the size of the battery system through the identification of the optimal value for the parameter α_k. This parameter represents the proportion of the PV peak

power of the system *k*, used to charge the storage system *k*. This parameter is comprised between 0 and 1.

$$f = \min \sum_{k=1}^{N} \alpha_k \cdot P_{PV,k} \tag{16}$$

Subject to:

$$\alpha_1, \alpha_2, \ldots \alpha_k = \alpha_1 \tag{17}$$

$$P_{bat.k}^{\min} \leq P_{bat,k} \leq P_{bat.k}^{\max} \tag{18}$$

From the above, *N* represents the total number of PV systems in the feeder; $P_{bat,k}^{\min}$ and $P_{bat,k}^{\max}$ are the limit values of power to which the storage system *k* can be activated, and $\alpha_k \cdot P_{PV,k}$ corresponds to the value of the power threshold, P_{th}, for each PV system operating. From (17), it is defined that the value of α_k is common for the whole system in each simulation case, to homogenise the activation of the storage systems (Table 9).

Once the value of P_{th} is determined, the battery system *k* stores the energy from the PV system *k*, charging it according to (19) which is the $P_{bat,ch(t)}$ parameter of (14).

$$P_{bat,ch,k(t)} = P_{PV,k(t)} - P_{th} \tag{19}$$

On the other hand, the magnitude of the discharge power of the storage system during peak time, $P_{bat,dis(t),}$ is in function of the amount of power coming from the grid to be shaved. Therefore, it can be defined as a percentage of the demand over time from (20) to be evaluated in (15). The value of σ is an empirical parameter, based on the number of hours for which the set of batteries will reach its minimum charge value as shown in Table 9.

$$P_{bat,dis(t)} = \sigma \cdot P_{laad(t)} \tag{20}$$

In accordance, it is defined that in every *t*, it must be fulfilled that the amount of energy of the battery bank, as well as the *SOC*, must be subject to the restrictions defined in (21) and (22).

$$E_{bat}^{\min} \leq E_{bat(t)} \leq E_{bat}^{\max} \tag{21}$$

$$SOC_{\min} \leq SOC_{(t)} \leq SOC_{\max} \tag{22}$$

According to (21) and (22), the maximum state of charge of the battery bank, SOC_{max}, will take the value of the nominal battery capacity, $E_{bat}^{\max}$, and the minimum state of charge of the battery bank, SOC_{min}, will be determined by the maximum depth of discharge, DOD, expressed in (13).

In this sense, as shown in Fig. 6 to Fig. 8, the battery control and activation algorithm embedding as a battery management algorithm for charging and discharging are shown:

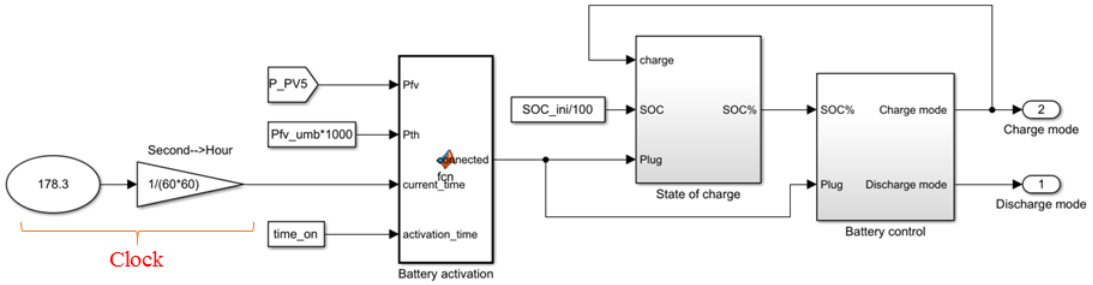

Fig. 6. Battery management algorithm

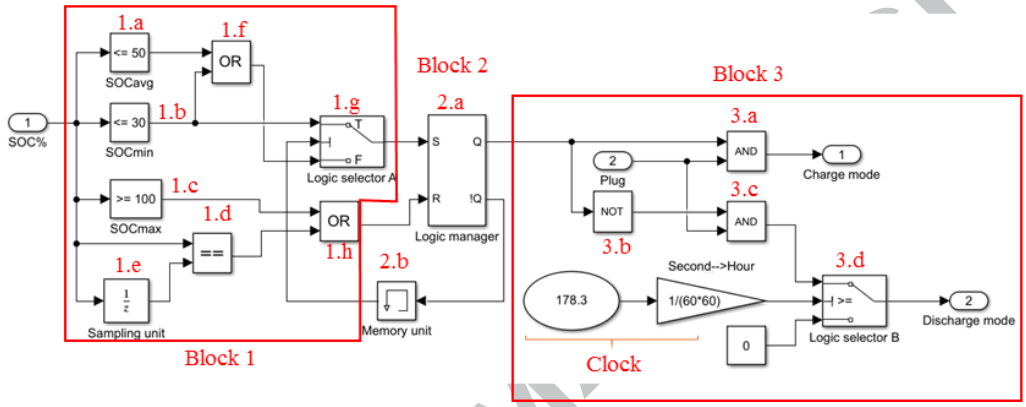

Fig. 7. The proposed battery control algorithm for charging/discharging

$$
\begin{aligned}
&\textit{If } P_{PV(t)} \geq P_{th} \textit{ OR Current time} \geq \textit{Activation time} \\
&\qquad \textit{Connected} = 1 \\
&\textit{Else} \\
&\qquad \textit{Connected} = 0 \\
&\textit{End}
\end{aligned}
$$

Fig. 8. The proposed BESS activation algorithm

From Fig. 6 during the system operation in each time step, the *Battery activation* block supervises as inputs $P_{PV(t)}$, P_{th}, the *current time* and the *activation time* (Table 10) to enable the port *connected* to hook up the BESS to the grid. These variables are managed to the proposed BESS activation algorithm, either by P_{th} or *activation time* as shown in Fig. 8. At the same time, considering the BESS initial *SOC*, the *State of Charge* block evaluates the *SOC* of the battery pack according to the equations set (11) to (15). This *SOC* is the input to the *Battery control* block in which is contained the proposed battery control algorithm for charging and discharging.

To better understand the operation of the battery control algorithm shows in Fig. 7, it has been divided into three blocks:

1) Once calculated the SOC, in the first block three comparators (*1.a*, *1.b* and *1.c*) verify this parameter is between 30% and 50% and besides, that this is not

greater than the SOC_{max}. The interval above represents the lower limit of discharge of the battery (SOC_{min}) and the average value at which the battery will be able to absorb enough energy to reach the SOC_{max}.

2) Employing a *sampling unit* (*1.e*), every 15 minutes the *SOC* is sampled and stored to be compared (*1.d*) with any change in its magnitude when charging or discharging occur. Therefore, before any condition of Fig .8 are met, the initial *SOC* will be the current *SOC* being one the output of *1.a, 1.b, 1.f, 1.d* and *1.h* and zero from *1.c*. Thus, the signal from *1.f* will pass through the *Logic selector A* (*1.g*) to input *S* of the *Logic manager* (*2.a*) in the block 2, while the signal from *1.h* is sent to input *R*. Hence, according to the last row of Table 3, *2.a* will be in idle mode. Plus, the *Memory unit* (*2.b*) works as selection criterion for (*1.g*) to evaluate the changes in the input of (*2.a*) based on $!Q \geq 0.5$.

3) When the $P_{PV(t)}$ is higher than P_{th}, the BESS activation algorithm sends the connection signal to the Plug ports of the State of charge and Battery control blocks of Fig. 6 (i.e., also to the input two of Fig. 7). This means that *2.a* operates according to the third row of Table 3, and the *Charge mode* port will enable the charging process because of the output of *3.a* is true. This signal is sent it back to the *State of charge* block only to verify the condition of activation as shown in Fig. 6. The charging process continues as long as $P_{PV(t)}$ is higher than the threshold power. When $P_{PV(t)}$ is less than P_{th}, and the *SOC* has reached its maximum value or one close to it, the *Logic manager* receives a false and true command at inputs *S* and *R*, respectively as the second row of Table 3. This action tells *2.a* to enables the discharging command making true the output of *3.b* and *3.c* of block 3. However, the *Discharge mode* port will be activated only when the clock coincides the scheduled connection time of the storage system (Table 10), allowing to the signal passes through the input one of the *Logic selector B* (*3.d*). The discharging process will continue until SOC reaches its minimum value. The first-row case of Table 3 will occur during the change from charging mode to discharging mode keeping the previous state outputs Q_{n-1} and $!Q_{n-1}$.

Table 3
Local manager for charging/discharging mode

S	R	Q	!Q	Command
0	0	Q_{n-1}	$!Q_{n-1}$	-
0	1	0	1	Discharging
1	0	1	0	Charging
1	1	0	0	-

4. Case study

This section analyses the outcomes of the proposed BESS management algorithm by integrating it with the installation of a series of PV systems connected to a BESS group, distributing them in each of the five load nodes of the network of Fig. 2. Each configuration of the PV+BESS will allow evaluating the impact these systems on the voltage deviation and losses of the system. In this way, five use cases have been

proposed for summer and winter scenario with the aim to find the minimum system losses possible and maximum voltage deviation in the last use case. This makes appropriate, due to each case corresponds to a particular increase in the percentage of the PV installed. I.e., by 23% [14], 50%, 75 %, 100% and 125% of the rated feeder capacity. From [23] is taken that the $\%PV_{integration}$ is in function of the $PV_{installed}$ power and their capacity factor (*CF*) as well as the feeder capacity, as expressed in (23). The rated feeder capacity has been considered as the capacity of the first line section on the LV side of the transformer, calculated by the technical specifications of [24], which corresponds to 285.45 kVA. The results for summer scenario are presented, as it is the one in which there is the most significant energy contribution from photovoltaic systems. The whole system has been modelled in MATLAB/Simulink making use of the quasi-static load flow calculation. Table 4 and Table 5 show the parameters used in the simulations.

$$\%PV_{integration} = \frac{CF \cdot PV_{installed}}{Utility_{capacity}} \cdot 100 \tag{23}$$

Table 4
Key parameters of PV system model

Parameter	Value	Reference
η_{panel}	0.14	[11]
η_{pc}	0.95	[11, 12]
η_{inv}	0.92	[11, 12]
β	0.005/°C	[2, 15]
NOCT	47°C	[11]
$T_{cell,ref}$	25°C	[11]

Table 5
Key parameters of BESS system model

Parameter	Value	Reference
$\eta_{bat,inv}$	0.92	[2, 30]
SOC_{min}	30%	[10, 30]
SOC_{max}	100%	[10, 30]
DOD	70%	-
Δt	1 min	-

After calculating the $PV_{installed}$ for each use case, this power was distributed in each load node as shown in Table 6. The P_{total} of case 1 was distributed according to the case study presented in [14]. The power distribution for the remaining four cases was made taking into account the ratio between the PV power of each node and the total installed PV power for case 1 multiplied by the P_{total} of the last row of Table 6. For instance, for case 2 the $PV_{installed}$ for node *R11* is *8.8/65.6 * 142.7 kWp* and sequentially for the remaining nodes and cases.

Table 6
Rated PV installed capacity per node and total for each simulation case

Node	Case 1 (23%)	Case 2 (50%)	Case 3 (75%)	Case 4 (100%)	Case 5 (125%)
R11	8.8	19.1	28.7	38.3	47.9

R15	7.7	16.8	25.1	33.5	41.9
R16	7.7	16.8	25.1	33.5	41.9
R17	20.7	45.0	67.6	90.1	112.6
R18	20.7	45.0	67.6	90.1	112.6
P_{total} [kWp]	65.6	142.7	214.1	285.5	356.8

From the simulations performed for the five cases, it was calculated that the capacity factor, *CF*, for this scenario was 0.54. In this way, from (23) the percentage of PV insertion was determined for each simulation case. These results are shown in Table 7.

Table 7
PV power generated per node according to $\%PV_{integration}$

Node	Percentage of PV integration				
	12%	27%	40%	54%	67%
	P_{PV} [kWp]				
R11	4.71	10.22	15.36	20.49	25.63
R15	4.12	8.99	13.43	17.92	22.42
R16	4.12	8.99	13.43	17.92	22.42
R17	11.08	24.08	36.17	48.21	60.25
R18	11.08	24.08	36.17	48.21	60.25
P_{total} [kWp]	35.11	76.36	114.56	152.75	190.97

To define the energy capacity of each BESS the value of the P_{th} was found initially for case 1 from the identification of the coefficient α, by means of (16) to (18), to determine the charging power of the batteries, $P_{bat,ch(t)}$. Moreover, the value of the coefficient σ was defined, adjusted to optimise the time of use of the batteries, and thus obtain the battery discharge power, $P_{bat,dis(t)}$.

Once these parameters were determined, the distribution of the energy capacity of the batteries, E_{bat}, was proposed in each loading node, as shown in Table 8. Based on this, the energy capacity of the batteries was scaled to different proportions in each node for the remaining cases of simulation, in such a way that values close to the SOC_{max} were reached during the charging process.

Table 8
Rated capacity of BESS per node and $\%PV_{integration}$

Node	Percentage of PV integration				
	12%	27%	40%	54%	67%
	E_{bat} [kWh]				
R11	20	40	40	50	62
R15	18	36	36	45	54
R16	18	36	36	45	54
R17	40	80	80	108	136
R18	40	80	80	108	136
$E_{bat, total}$ [kWh]	136	272	272	356	442

As shown in Table 9, the value of the coefficient α increases its magnitude only up to 40% of PV penetration, as the capacity of the PV generation system increases. However, it remains constant for the following percentages of penetration, in order to reduce the capacity of the storage system and maximise the period of discharge. That is why two values were set for the coefficient σ that met these requirements.

Table 9
Value of α and σ for each $\%PV_{integration}$

Percentage of PV integration	α	σ
12%	0.26	0.08
27%	0.3	0.1
40%	0.32	0.1
54%	0.32	0.1
67%	0.32	0.1

4.1. Technical losses

Fig. 9 shows the evolution of the average losses for the summer scenario of the five simulation cases, respectively. The first result that demands attention is the shape of the graph. Losses begin to decrease as the PV integration index increases, until before its minimum level is reached. To demonstrate that the behaviour of the losses presents a U-shaped trajectory, as studied in [23], an adjustment was made to the data of the simulated cases by means of a quadratic polynomial which was adapted as expected to the possible cases where the percentage of FV insertion will continue to increase, as seen in both views of Fig. 9.

Thus, it is observed in view (b), that once the minimum value of losses is reached if the level of FV insertion continues to increase, then the losses will begin to increase marginally as well. Also, if the PV insertion level increases enough, the losses can be even more significant than without the connected PV+BESS.

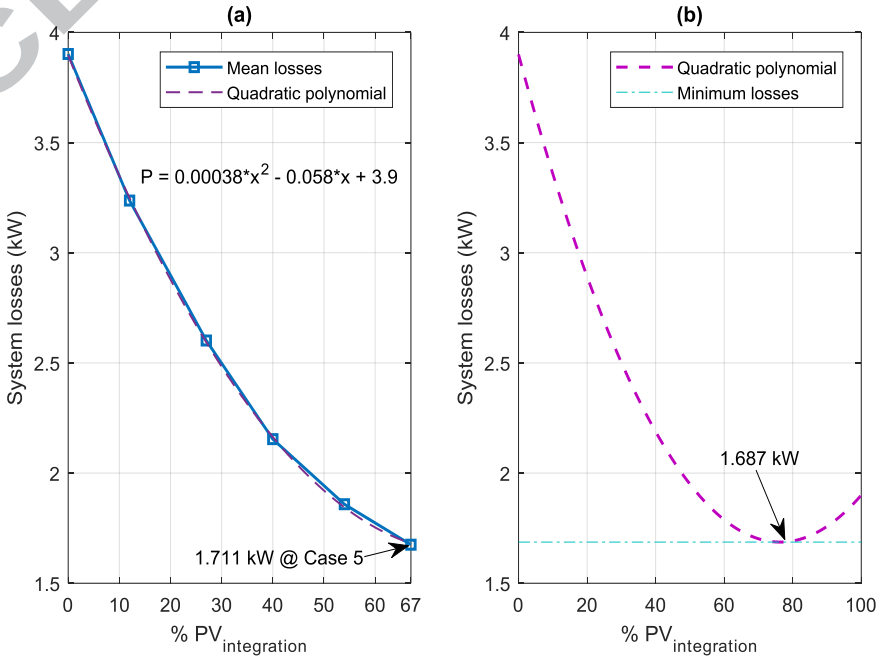

Fig. 9. a) Power system losses in summer scenario for the five integration cases of PV+BESS. b) Adjusting quadratic polynomial for losses.

Likewise, for the two views of Fig. 9, in the last case of simulation, the average losses of the system approximate the minimum losses found by the polynomial adjustment made. This finding corroborates what is presented in [1], where the Fraunhofer Institute calculates that up to 66% more photovoltaic solar energy can be installed in a given area, in circumstances in which the peak of this generation is not exported to the grid. This scenario is possible, mainly when the solar power to the network is restricted, and the supply of the battery corresponds to the demand of the users.

4.2. BESS operation with the energy management system algorithm

As already mentioned, the BESS charging is a function of a threshold power value that depends on the α coefficient and the installed PV nominal power. Therefore, the activation time will be a function of the instant in which such value of P_{th} is exceeded. However, the activation of the storage system discharge can be controllable (Fig. 6 to Fig. 8). For this, it was proposed that the BESS of each node should operate according to the schedules presented in Table 10. The selection of such time intervals is because, with these, the optimum operation of the storage set occurs to reduce the technical losses of the system and to reduce the power contributed by the network, for a specific σ coefficient.

Considering the above, in views (a) through (e) of Fig. 10, the *SOCs* are shown by the percentage of PV insertion and storage capacity, in the five load nodes, for the five cases of simulation in the summer scenario. The magnitude of the coefficient α varies for each simulation case. In this way, the charging process of the storage systems starts from 9:00 h and 10:00 h, as seen in views (a), (b) and (c).

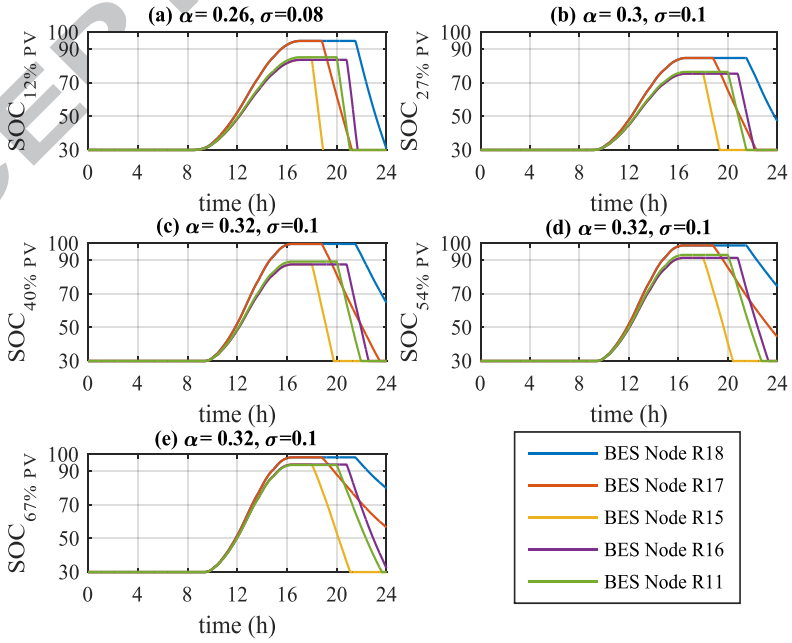

Fig. 10. *SOC* by $\%PV_{integration}$ and storage capacity on the load nodes

Furthermore, it is observed that in all the simulation cases *SOC* values close to the maximum capacity are reached. This outcome means that the capacity of the storage systems was suitably sized to accumulate the energy coming from the PV generation with the obtained α coefficients.

Table 10
BESS activation time for discharging in summer scenario

Node	Hour of the day Summer
R11	20:00
R15	18:00
R16	20:48
R17	18:48
R18	21:30

Besides, storage systems are discharged at 30% capacity with the aim of not reduce the useful life of them by deep discharges. Also, it specifies that the start time of discharge corresponds to the content in Table 10, allowing the discharge of each BESS is not made suddenly but there is mutual support between each node, to optimise the use of battery capacity, and thus, cover most of the peak demand period.

4.3. Resultant voltage and power profiles

To examine the behaviour of the voltage profiles throughout the day for the different simulation cases the base case was taken as the reference without the insertion of the PV+BESS. Thus, the view (a) of Fig. 12 shows the RMS voltage level of all the nodes of the network, ordered according to the topology of the system, for a simulation period of 24-h. In node 15 at noon, the lowest voltage magnitude of the grid is presented, but it remains above the admissible 0.93 p.u. [25]. The earlier is because this node is not located equidistantly from the main feeder compared to the other four load nodes. Therefore, the voltage drop that is generated in the conductors is greater. Added to this such node represents the second largest load connected to the feeder.

Likewise, the percentage of reduction of the average power imported from the network, $\%P_{reduction}$, has been evaluated, thanks to the connection of the PV+BESS according to (24). Where μ_{Pfinal}, refers to the mean value of the power of the case *k*, and $\mu_{Pbase\ case}$, refers to the average power of the summer scenario. The results obtained are summarised in Table 11 for each study case.

$$\%P_{reduction} = \left(1 - \frac{\mu_{Pfinal}}{\mu_{Pbase\_case}}\right) \cdot 100 \tag{24}$$

Table 11
Percentage reduction of the mean $P_{base\ case}$ for summer, compared to the mean P_{final} for all five cases of simulation

$\%PV_{integration}$	12%	27%	40%	54%	67%
$\%P_{reduction}$	9.5%	20.5%	30.7%	40.1%	49.3%

Taking into account the above, the results of the simulation cases 1 and 5 with the percentages of PV insertion and capacity of the corresponding BESS are presented below.

4.4. Case 1

Fig. 11 shows the apparent power decomposed in its real and reactive components. These profiles are the result of having integrated 12% of PV generation with a 136 kWh BESS. To show the variation of the active power of the system the demand profile of the base case has been drawn. Likewise, the generated PV power curve is presented, where it is indicated that the level of P_{th} from which the storage system begins to load. The shaded area in yellow represents the energy stored in the BESS.

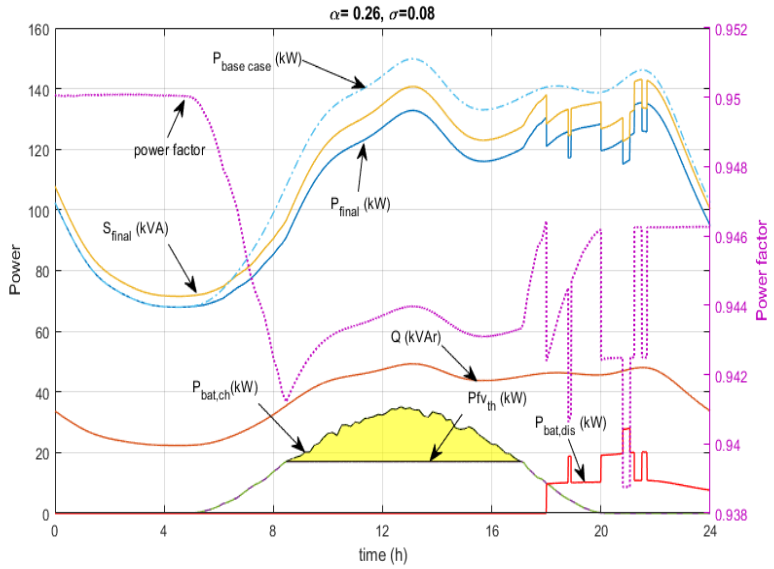

Fig. 11. Summer profiles for PF, P_{Demand}, 12% PV, 136 kWh BESS with α=0.26 and σ=0.08.

The red curve shows the profile of the discharge power from all the BESS, which along with the added PV power, reduce the contribution of the network by 9.5% respect to the base case. This result is because the storage systems reached SOCs close to the maximum, thanks to the fact that there was sufficient PV production.

The above is reflected in the behaviour of the power factor, where it can be seen that as the generated PV power increases, this begins to depreciate to the point when the BESSs start charging. Subsequently, it increases as the demand grows and the BESSs charging continue. Then, it varies again in a range of not less than 0.938, when the storage systems begin to discharge. However, at the end of the simulation period, the power factor remains at a value lower than 0.95 because the BESS of the R18 node has not reached the SOC_{min}. The variation of the power factor is because both the PV system and the storage systems only produce active power, while the network continues to provide the same reactive power as the base case.

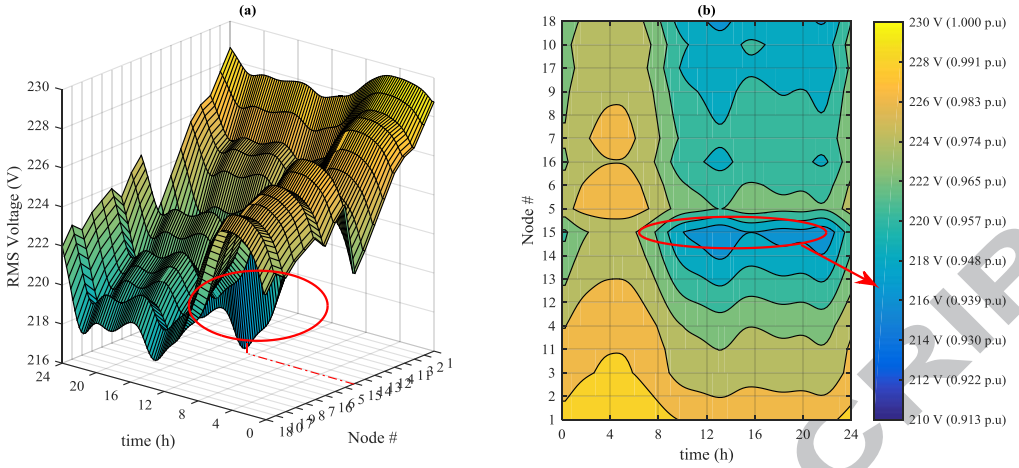

Fig. 12. Voltage profile for base case (summer)

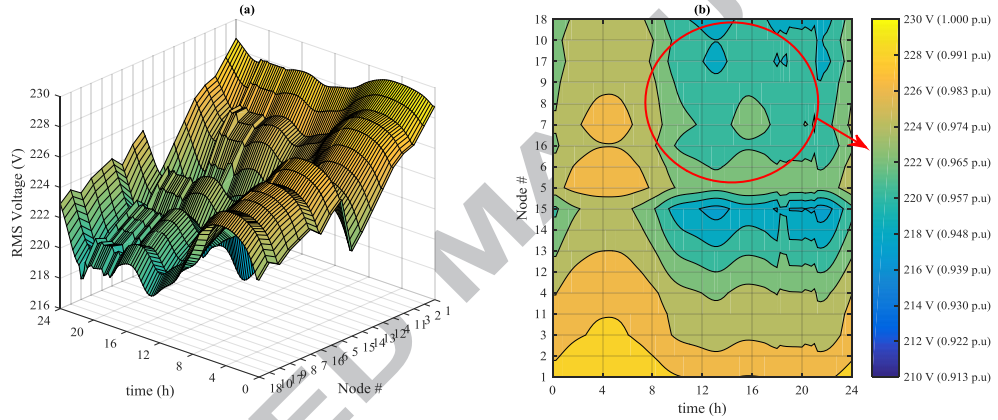

Fig. 53. Voltage profile for case 1 (summer), 12% PV, 136 kWh BESS with α=0.26 and σ=0.08

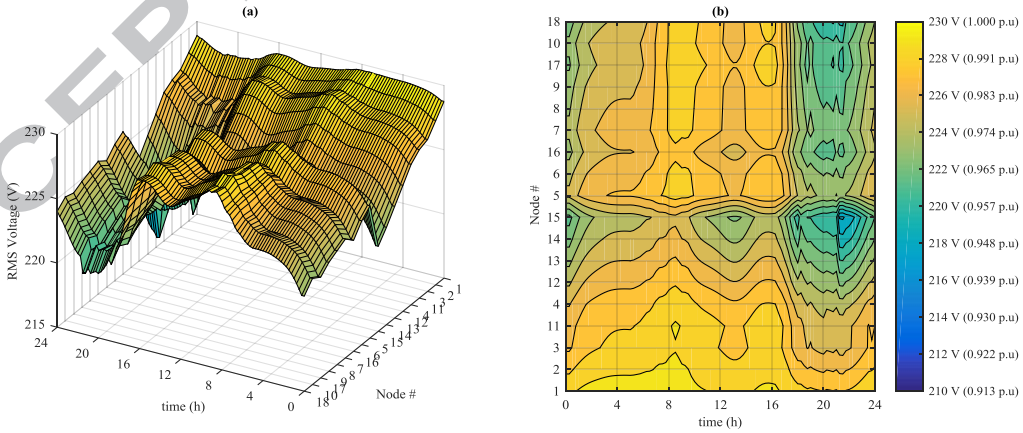

Fig. 14. Voltage profile for case 5 (summer), 67% PV, 442 kWh BESS with α=0.32 and σ=0.1

In response to the variation of the demand profile, voltage profiles similarly vary as shown in Fig. 13. If this figure is compared with Fig. 12 of the base case, it is observed, for instance, that for the area marked in view (b), the voltage levels of nodes 8 through 18 are now above 0.965 p.u. for approximately 16-h. Also, for node 15 the voltage is in the range of 0.957 p.u. for a similar time interval.

4.5. Case 5

Fig. 15 shows the apparent power decomposed in its real and reactive components. These profiles are the result of having integrated 67% of PV generation with a BESS of 442 kWh. Likewise, the profiles of generated PV power and power delivered by the BESSs to all load nodes are shown. The PV generation shows that its production is higher than the energy demanded by the load. However, thanks to the storage systems connected to the network, the possible surplus of energy, corresponding to the area highlighted in yellow, is stored which means that more than 50% of the PV power is supplied to the load. In this way, after 18:00 h, the stored energy is dispatched with the purpose of reducing the level of demand towards the network, which results in the fact that, at the end of the simulation period, the active power level of the network has been reduced by 49.3% with respect to the base case.

As in case 1, and in the subsequent ones, the network continues to provide the reactive power needed to maintain a power factor of 0.95. However, for this case, the magnitude of reactive power is higher than the active power by the power supplied from the PV systems, which causes the power factor to fall sharply to a value close to 0.6. However, it increases its value gradually when the BESSs start to charge, and it recovers again to values close to 0.95 when the PV production decreases, and the BESSs go into discharging mode.

From the above, it can be drawn that users depend on the reactive power provided by the network, although the network operator cannot bill for this service. This effect has two consequences: first, users cannot become independent of the network until they overcome reliance on reactive power; second, the network operator must schedule the generation to provide reactive power, although residents do not pay for it to maintain the power factor close to 0.95.

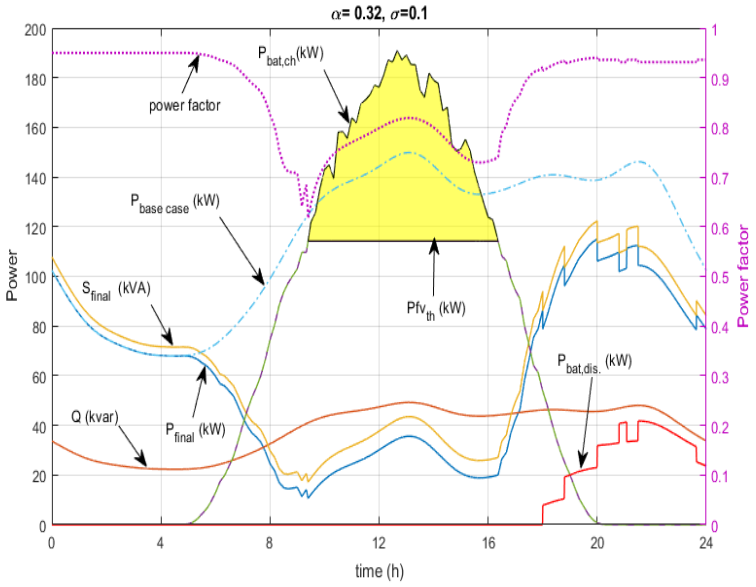

Fig. 15. Summer profiles for PF, P_{Demand}, 67% PV, 442 kWh BESS with α=0.32 and σ=0.1

Consequently, the variation of the voltage level in all the nodes of the network during the simulation period is shown in Fig. 14. In the view (a) of the same figure, the voltage

level that predominates during the hours of high irradiance is in the range of 0.983 p.u. to 1 p.u. respect to the base case of Fig. 12. However, it falls below 0.983 p.u. during the discharge of the storage systems, but it remains above 0.957 p.u. This behaviour is because the amount of energy coming from the PV+BESS is considerable enough to modify the contribution to the demand profile.

Having described the results obtained for cases 1 and 5, corresponding to the minimum and maximum percentage of PV insertion with storage, Fig. 16 shows the curves representing the maximum voltage deviation that exists between the nodes of the network in function of time, respect to the base case when the PV+BESS are connected, and its percentage of insertion is increased. These results were determined using the voltage deviation index, *VDI*, presented in [26] and expressed in (25); where $V_{\max}^{o}$ and $V_{\min}^{0}$ refer to the maximum and minimum voltage levels over time of the entire network, expressed in p.u., for the base case of both scenarios, while $V_{\max}^{k}$ and $V_{\min}^{k}$ refer to the maximum and minimum voltage levels in the time of the whole network, expressed in p.u., for the case k. In this sense, positive values of *VDI* involve a flattening of the voltage profile, while negative values imply a wider voltage deviation. From this, it is clear that in both figures only positive values of *VDI* are appreciated, because, for all simulation cases, the voltage does not exceed the 1 p.u.

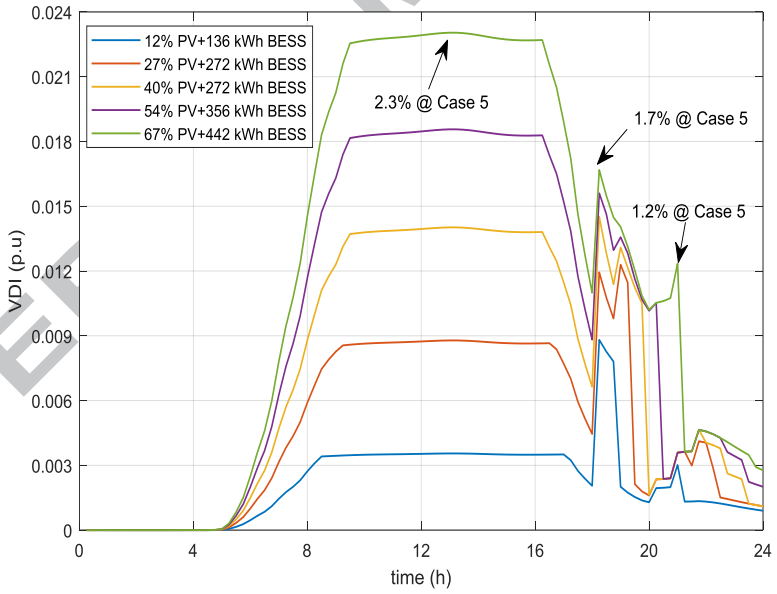

Fig. 66. VDI in time resulting from the integration of PV+BESS for each simulation scenario

$$VDI = \left(V_{\max}^{o}(t) - V_{\min}^{o}(t)\right) - \left(V_{\max}^{k}(t) - V_{\min}^{k}(t)\right) \quad (25)$$

For example, for the maximum percentage of insertion, the maximum voltage deviation is reached for the hours of energy contribution of the PV system, oscillating above 2.3%. Subsequently, this deviation decreases as the PV generation decreases, but increases again to 1.7% due to the action of the storage system. Finally, a second increase in the deviation is presented above 1.2%, due to the operation of the storage system of the node R18.

In this way, it is possible to show, as a guide, the behaviour of the voltage as a function of time over the whole system, for the period of simulation evaluated, and thus determine if the integrated generation-storage systems represent a benefit or harm to the network.

5. Conclusion and future work

The model developed for the storage system based on the limit operation of lead-acid batteries can be used to evaluate the behaviour of any electrochemical storage technology, because what varies are the parameters of the element behind the power converter.

The implemented strategy of control and management of the BESS improves the traditional way of controlling this type of systems in networks with installed PV systems, where the charge of the batteries is activated according to an optimised power threshold, instead of $P_{PV}>P_{Load}$. Likewise, this strategy allows to reduce the technical losses of the distribution system and to improve the behaviour of the voltage in the nodes at the end of the feeder, in comparison with the scenario without BESS+PV.

It was demonstrated that a high insertion of PV generation, even with storage, in the nodes where the demand is concentrated, pose challenges to the electrical infrastructure with radial topology. Because the mode of injection of energy from this type of technologies generates the conditions to produce a low power factor and, therefore, results in low active power demands as seen in this work. Also, the network operator must program and provide the reactive power necessary to maintain the balance of the system, even if the user is not billed.

As future work, the battery model, as well as the PV model, will be tested in an HIL simulation to validate its behaviour integrating the proposed BESS management algorithm. Moreover, studies on the BESS that consider weak grid dynamics including the integration of the EV and other renewable energy sources will be carried on.

Acknowledgements

The authors would like to thank the University of the Basque Country and TECNALIA for supporting the work done at the University of the Basque Country under research grant by the Carolina Foundation.

References

[1] International Renewable Energy Agency, "Battery Storage for Renewables: Market Status and Technology Outlook," IRENA, Abu Dhabi, 2015.

[2] A. Kaabeche, M. Belhamel and R. Ibtiouen, "Techno-economic valuation and optimization of integrated photovoltaic/wind energy conversion system," *Solar Energy*, vol. 85, no. 1, pp. 2407-2420, 2011.

[3] M. Gitizadeh and H. Fakharzadegan, "Battery capacity determination with respect to optimized energy dispatch schedule in grid-connected photovoltaic (PV) systems," *Energy*, vol. 65, pp. 665-674, 2014.

[4] C. Rus-Casas, J. Aguilar, P. Rodrigo, F. Almonacid and P. Pérez-Higueras, "Classification of methods for annual energy harvesting calculations of photovoltaic generators," *Energy Conversion and Management*, vol. 78, no. 1, pp. 527-536, 2014.

[5] J. A. Hernández Mora, "Methodoloy for the technical analysis of the massification of photovoltaic systems as an option of distributed generation in low voltage networks," PhD thesis, Engineering Dep., Universidad Nacional de Colombia, Bogotá, 2012.

[6] T. Markvart, Solar Electricity, England: John Wiley & Sons, 2000.

[7] M. Z. Daud, A. Mohamed, M. Z. Che Wanik and M. A. Hannan, "Performance Evaluation of Grid-Connected Photovoltaic System with Battery Energy Storage," in *IEEE International Conference on Power and Energy (PECon)*, Kota Kinabalu Sabah, Malaysia, 2012.

[8] V. Kalkhambkar, R. Kumar and R. Bhakar, "Optimal Sizing of PV-Battery for Loss Reduction and Intermittency Mitigation," in *IEEE International Conference on Recent Advances and Innovations in Engineering (ICRAIE-2014)*, Jaipur, 2014.

[9] CIGRE, "Benchmark Systems for Network Integration of Renewable and Distributed Energy Resources. Task Force C6.04.02," CIGRE, Paris, 2014.

[10] M. Castillo-Cagigal, E. Caamaño-Martín, E. Matallanas, D. Masa-Bote, A. Gutiérrez, F. Monasterio-Huelin and J. Jiménez-Leube, "PV self-consumption optimization with storage and Active DSM for the residential sector," *Solar Energy*, vol. 85, no. 9, pp. 2338-2348, 2011.

[11] M. Bortolini, M. Gamberi and A. Graziani, "Technical and economic design of photovoltaic and battery energy storage system," *Energy Conversion and Management*, vol. 86, no. 1, pp. 81-92, 2014.

[12] C. J. Rydh and B. A. Sandén, "Energy analysis of batteries in photovoltaic systems. Part I: Performance and energy requirements," *Energy Conversion and Management*, vol. 46, no. 11-12, pp. 1957-1979, 2005.

[13] M. Gitizadeh and H. Fakharzadegan, "Effects of electricity tariffs on optimal battery energy storage sizing in residential PV/storage systems," in *International Conference on Energy Efficient Technologies for Sustainability (ICEETS)*, Nagercoil, 2013.

[14] F. Marra, G. Yang, C. Træholt, J. Østergaard and E. Larsen, "A Decentralized Storage Strategy for Residential Feeders With Photovoltaics," *IEEE Transactions on Smart Grid*, vol. 5, no. 2, pp. 974-981, 2014.

[15] G. Tina and P. Scandura, "Case study of a grid connected with a battery photovoltaic system: V-trough concentration vs. single-axis tracking," *Energy Conversion and Management*, vol. 64, no. 1, pp. 569-578, 2012.

[16] D. Bi, S. Wang, . B. Ge and X. Yang, "Control Strategy of Grid-connected Photovoltaic System with Energy Storage," in *International Conference on Electrical Machines and Systems (ICEMS)*, Beijing, 2011.

[17] S. Jiang, W. Wang, H. Jin and D. Xu, "Power Management Strategy for Microgrid with Energy Storage System," in *37th Annual Conference on IEEE Industrial Electronics Society*, Melbourne, VIC, 2011.

[18] Basque Energy Agency, "Energy keys of the domestic sector," EVE, Bilbao, 2013.

[19] State Agency Official State Gazette, "BOE-A-2014-13617," The government of Spain - Presidency Ministry, Madrid, 2014.

[20] A. Newbery, "Trigonometric Interpolation and Curve-Fitting," *Mathematics of Computation*, vol. 24, no. 112, pp. 869-876, 1970.

[21] Basque government, "Open Data Euskadi," 2011. [Online]. Available: http://opendata.euskadi.eus/w79-resformx/es?r01kQry=tC:euskadi;tF:opendata;tT:ds_meteorologicos;m:documentLanguage.EQ.es;p:Inter. [Accessed 07 2017].

[22] D. Rekioua and E. Matagne, "Cahpter 5. Modeling of Storage Systems," in *Optimization of Photovoltaic Power Systems Modelization, Simulation and Control*, London, Springer, 2012, pp. 149-179.

[23] V. Quezada, J. Abbad and T. San Román, "Assessment of energy distribution losses for increasing penetration of distributed generation," *IEEE Transactions on Power Systems*, vol. 21, no. 2, pp. 533-540, 2006.

[24] KMI Wire and Cable, "LV Power cables NA2XSY 1 x (10-800) mm² 0.6/1 kV," 28 09 2011. [Online]. Available: http://kmiwire.com/products/lv-power-cables/aluminium-cables/131.html. [Accessed 07 2015].

[25] M. o. Economy, "RD 1955/2000, Art. 104.3," BOE, Madrid, 2000.

[26] F. M. Gonzalez-Longatt and J. L. Rueda, "Chapter 6. Assessing the Renewable Energy Sources Integration Through a Series of Technical Performance Indices Using DIgSILENT PowerFactory DPL," in *Power Factory Applications for Power System Analysis*, Switzerland, Springer, 2014, p. 139.

[27] Xiaohua Wu, Xiaosong Hu, Scott Moura, Xiaofeng Yin and Volker Pickert, " Stochastic control of smart home energy management with plug-in electric vehicle battery energy storage and photovoltaic array," *Journal of Power Sources*, vol. 333, pp. 203-212, 2016

[28] Xiaohua Wu, Xiaosong Hu, Yanqiong Teng, Shide Qian and Rui Cheng, "Optimal integration of a hybrid solar-battery power source into smart home nanogrid with plug-in electric vehicle," *Journal of Power Sources*, vol. 363, pp. 277-283, 2017

[29] Xiaosong Hu, Changfu Zou, Caiping Zhang, and Yang Li, "Technological Developments in Batteries - A Survey of Principal Roles Types and Management Needs ," *IEEE Power & Energy Magazine*, vol. 15, no. 5, pp. 20-31, 2017

[30] Raul V.A. Monteiro, Geraldo C. Guimarães, Fabricio A.M. Moura, Madeleine R.M.C. Albertini and Fernando B. Silva, "Long-term sizing of lead–acid batteries in order to reduce technical losses on distribution networks: A distributed generation approach," *Electric Power Systems Research*, vol. 144, pp. 163-174, 2017

[31] Sherif A. Abdelrazek, and Sukumar Kamalasadan, "Integrated PV Capacity Firming and Energy Time Shift Battery Energy Storage Management Using Energy-Oriented Optimization," *IEEE Transactions on Industry Applications*, vol. 52, no. 3, pp. 2607-2617, 2016

[32] Wei Jiang, Lei Zhang, Hui Zhao, Huichun Huang and Renjie Hu, "Research on power sharing strategy of hybrid energy storage system in photovoltaic power station based on multi-objective optimisation," *IET Renewable Power Generation*, vol. 10, no. 5, pp. 575-583, 2016

[33] Adel Merabet, Khandker Tawfique Ahmed, Hussein Ibrahim, Rachid Beguenane and Amer M. Y. M. Ghias, "Energy Management and Control System for Laboratory Scale Microgrid Based Wind-PV-Battery," *IEEE Transactions on Sustainable Energy*, vol. 8, no. 1, pp. 145-154, 2017

[34] B. S. Borowy and Z. M. Salameh, "Methodology for optimally sizing the combination of a battery bank and PV array in a wind/PV hybrid system," *IEEE Transactions on Energy Conversion*, vol. 11, no. 2, pp. 367-375, 1996

Highlights

1. The demand is evaluated by the trigonometric interpolation method.
2. A suitable control strategy optimised the BESS charging/discharging process.
3. Users depend strongly on the network reactive power.
4. Voltage and losses magnitude improve by PV+BESS penetration level.